Desalination and Water Treatment
www.deswater.com

doi: 10.5004/dwt.2020.25677

193 (2020) 19–33
July

Improvement of cellulose acetate forward osmosis membrane performance using zinc oxide nanoparticles

Mostafa El-Noss[a], Heba Isawi[a], Hossam A. Shawky[a,*], M.A. Gomaa[b], M.S.A. Abdel-Mottaleb[c]

[a]*Egyptian Desalination Research Center of Excellence (EDRC), Desert Research Center, Cairo, Egypt, email: shawkydrc@hotmail.com (H.A. Shawky)*
[b]*Hydro-geochemistry Department, Desert Research Center, Cairo, Egypt*
[c]*Chemistry Department, Faculty of Science, Ain Shams University, Abbassia, Cairo, Egypt*

Received 6 December 2019; Accepted 12 February 2020

ABSTRACT

With the continual progress in developing the forward osmosis (FO) membrane, in both industry and academia, it is prospected to remain the best alternative technique for the production of freshwater. The current paper focuses on the preparation and characterization of FO membranes and ZnO nanoparticles (ZnO NPs) that can be used for membrane modification to enhance its performance. FO membranes are fabricated in our labs from the cellulose acetate (CA) polymer by phase inversion methods. These membranes are easy to prepare, stable against bacterial attack, chemical, and mechanical changes, as well as showing excellent performance and superior economics. The optimum conditions for preparing forward osmosis cellulose acetate (FO-CA) membranes are; 7 wt.% CA, 92.75 wt.% acetone, and 0.25 wt.% ZnO NPs per unit percentage of CA in aqueous solution. A new approach for the modification of CA membranes using the synthesized ZnO NPs was shown to enhance the performance of membranes for forward osmosis water desalination process. We study the effect of polymer concentration, membrane thickness, and membrane modification by ZnO NPs on membrane performance. The fabricated membranes were characterized by X-ray diffraction (XRD), scanning electron microscopy (SEM), attenuated total reflectance–Fourier transform infrared spectroscopy, and the mechanical properties were studied in order to expose the best membrane for water desalination and also the synthesized ZnO NPs were characterized by XRD and SEM. The performance of the CA/ZnO NPs membranes were examined using parameters, such as contact angle, surface area and pore size, water flux (J_w), and salt rejection (R%). Compared with the pure CA membrane, the CA membrane modified with ZnO NPs was more hydrophilic, with an improved water contact angle (~47.6 ± 2°) over the pure CA membrane (~63.85 ± 2°) and it showed improving in water flux (26.57 L h^{-1} m^{-2}) over the pure CA membrane (19.42 L h^{-1} m^{-2}), also it showed salt rejection 99.5% of Na^+, 100% of Cl^-, and 99.6% of Mg^{2+}. The water flux increased in the case of CA membrane modified with ZnO NPs is due to increasing in surface area and total pore volume than the pure CA membrane by 23% and 20%, respectively. This demonstrates that the CA membrane modified with ZnO NPs can significantly improve the membrane performances and was suitable to enhance the selectivity, and water flux of the membranes for water desalination.

Keywords: Forward osmosis; ZnO NPs; Cellulose acetate; Surface area; Salt rejection

* Corresponding author.

Presented at the 4th International Water Desalination Conference: Future of Water Desalination in Egypt and the Middle East, 24–27 February 2020, Cairo, Egypt

1. Introduction

General water crisis and fresh water scarcity are those of the most serious challenges during the last decades. Nowadays, the desalination process has a noticeable position in addressing the challenges [1]. Major interests expressed in the desalination of water using reverse osmosis (RO) are (1) high applied hydraulic pressures to produce the driving force for osmosis results in high energy consumption, (2) environmental problems in the drainage of concentrated brine, and (3) operational costs in the replacement of membrane. For any new desalination technology to be commercially applicable it must offer considerable improvements over RO in at least one of many performance measures. Because of the absence of external hydraulic pressure, FO has several unique advantages in terms of low energy consumption, efficient water recovery, low membrane fouling, and easy fouling removal, compared with conventional pressure-driven membrane processes such as RO, nanofiltration (NF), and ultra-filtration (UF) [2]. Due to these reasons, FO has attracted massive attention within the membrane community which sees research efforts intensifying over the past decade, especially within the last 8 y (Fig. 1).

Forward osmosis (FO) for desalination exhibit with the promise of overcoming the challenges of pressure-driven membrane processes. FO uses a semi-permeable membrane to separate water from dissolved salts similar to reverse osmosis process [4]. The semi-permeable membrane works as a barrier that permits small molecules such as water to pass through while blocking larger molecules. In this process, a concentrated solution owns higher osmotic pressure (draw solution) than the feed is circulated on the permeate side of the membrane. The osmotic pressure gradient across the membranes acts as the driving force for the transfer of pure water through the membrane. FO operates at low pressures, gives high rejection of dissolved solutes and provides low fouling propensity [2]. The main challenges in the FO process are the selection of a suitable osmotic agent to make draw solution and preparation of effective membranes which offer high water flux, high salt rejection with no internal concentration polarization (ICP). Another area of interest in the FO process is the recovery of pure water from draw solution which depends upon the performance of the membranes and draw solute used. The main contributing factors for the success of this membrane are the relative thickness of the membrane and the internalisation of fabric support layer. Various draw solutes and their recovery have been reported in literature, but only few of them could be considered acceptable in terms of recovery and energy requirements [4]. Keeping in view of the high fluxes and detention of solutes in nanofiltration separation process, nanofiltration (NF) might reduce the energy consumption in the recovery of pure water. The recovery of pure water, reuse of draw solution and the energy consumption in the combined FO and NF process will determine if FO can be an alternative to RO or not. However, due to the low permeability of the current FO membranes the FO-NF process needs far greater membrane area than RO, but at the same time the equipment cost will not be as high because FO is carried out at atmospheric pressure. Membranes offering high mechanical strength, fluxes, salt rejections, and low ICP are fatal for the commercial success of FO. However, the lack of effective membranes had disturbed FO development. In this regard, many researches condensed on FO membrane development during last decade. Different types of FO membranes including phase-inversion, thin-film composite and layer-by-layer have been fabricated [5–13]. Usually, a high performance FO membrane requires (1) a thin selective layer with high water permeability as well as low solute permeability, (2) a highly porous and hydrophilic support layer with proper water transport as well as low ICP, and (3) valuable anti-fouling properties [14–16]. Different kinds of relatively costly materials have been applied to prepare FO membranes such as polysulfone [11,17], polyethersulfone [13,18], and their sulfonated materials [7,8,12,19]. Since cellulose-based membranes have actual advantages including low cost, wide availability, high hydrophilicity, low fouling, and excellent chlorine resistance, cellulose esters are alternative materials in the fabrication of FO membranes [20,21].

The object of this paper is developing new cellulose based membranes to enhance the FO process performance. One approach to this objective is optimizing the composition of casting solution and preparation conditions of the FO membrane. In this paper nanotechnology along with membrane science has been applied to build a high-performance FO membrane. The work reports the effect of polymer concentration, membrane thickness, and the addition of ZnO NPs on water flux and salts rejection in

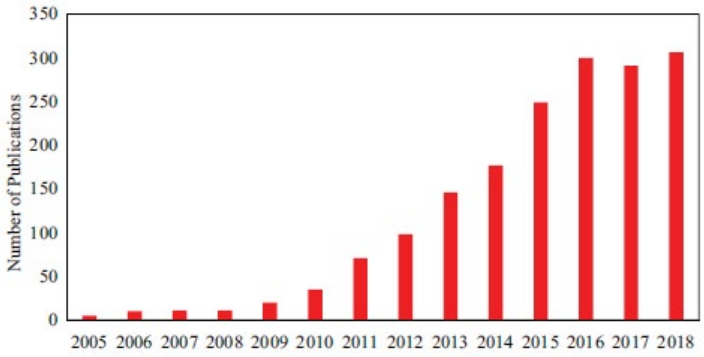

Fig. 1. FO publications since 2005 (based on SCOPUS database) [3].

the FO process. Membranes are tested in FO processes using anhydrous magnesium sulphate as the draw solute which can be separated by nanofiltration for reuse. Hybrid inorganic nanocomposite membranes are promising materials in FO application. The incorporation of inorganic nanoparticles in membranes can result significant changes in the membrane properties such as surface morphology, surface area, hydrophilicity, and FO performance [15,22–24]. It is worth mentioning that the physical and chemical properties of the membrane matrix can be tailored by the choice of the inorganic nanoparticles. In this regard, ZnO NPs as hydrophilic inorganic nanoparticles were selected to improve the cellulose-based membrane structure, surface properties, and performance [25].

2. Materials and methods

2.1. Chemicals

All reagents were of pure or analytical grade (Aldrich and Fluka, Germany) and were used as received. The solutions were prepared with pure distilled water. Cellulose acetate (CA) with 39.7 wt.% acetyl content with an average molecular weight of 52,000 g mol^{-1} (Aldrich) was used as the polymer forming membrane. Polyvinylpyrrolidone M.W. 3500 (PVP-K12), anhydrous zinc chloride, sodium lauryl sulfate (SLS), anhydrous magnesium sulfate and sodium chloride were purchased from Sigma-Aldrich, (Germany). Acetone HPLC with an analytical purity of 99.9% (Aldrich) and distilled water was used as the solvent and non-solvent, respectively. Nonwoven support with a thickness of 90 μm, obtained from PHILOS Co., Ltd., Korea was used as backing to cast membranes.

2.2. Synthesis of ZnO nanoparticles

The ZnO nanoparticles were synthesized using the hydrothermal method, which does not require the use of organic solvents and can be considered an environmentally friendly technique [26]. Three grams of zinc chloride was dissolved in 20 mL of distilled water. Sixteen milliliters of a 5 M NaOH solution was added drop wise to the zinc chloride solution while gently stirring for a period of 60 min at 50°C. During this period, 1.5 g of SLS was dissolved in 15 mL of distilled water and was added to the zinc chloride mixture. SLS, as a surfactant, plays an important role in the modification of the ZnO particles, and acts as an insulator between the nanoparticles, allowing them to overcome the interacting forces between them to create a homogeneous dispersion. A white precipitate appears immediately upon mixing the zinc chloride solution. The mixture was moved to a Teflon stainless steel autoclave (volume 80 mL) and filled with deionized water up to 80% of the reactor volume for hydrothermal treatment at 120°C for 5 h. The autoclave was then allowed to cool down naturally. The suspended ZnO nanoparticles were centrifuged at 6,000 rpm for 15 min and collected as a white precipitate. The precipitates were washed three times with distilled water and then ethanol to remove impurities. They were then dried at 50°C for 5 h and stored.

2.3. Preparation of FO membranes by phase inversion

CA/ZnO flat sheet membranes were prepared by the phase inversion method. Fig. 2 shows the membrane formation process. Nonwoven support was pasted to the glass plate using 10 wt.% polyvinylpyrrolidone (PVP-K12) solution in water. In order to prepare membranes, a dope solution of CA was prepared. At first ZnO nanoparticles were mixed with acetone and stirred for 2 h. The mixture was sonicated for 3 h in sonication cell to ensure a homogeneous spread of the nanoparticles. Then CA (7 wt.% by weight of the solution) was added to the initial mixture in three 30 min intervals and dissolved in the solvent. The concentration of ZnO nanoparticles added to CA were varied from 0 to 0.5 wt.% per unit percentage of CA. Then the mixture stirring for 8 h to has optimal dispersions of the nanoparticles in the polymer solutions. The casting solutions were then kept for 24 h to remove air bubbles. After that, the casting solutions were cast on a glass plate using automatic film applicator in a thickness of 50 μm. The membrane was allowed to dry and the solvent was slowly evaporated in an air for a suitable time (1 min). The cast films were subsequently immersed for 5 min in a distilled water bath with a temperature of 4°C to complete the phase separation process, where the exchange between the solvent and non-solvent was stimulated. Finally, the membranes were heat-treated in a distilled water bath at 70°C for 20 min to remove the excess acetone. The synthesized membranes were kept in a container of deionized water to be ready for characterization. The thickness of all the membranes is in the range of

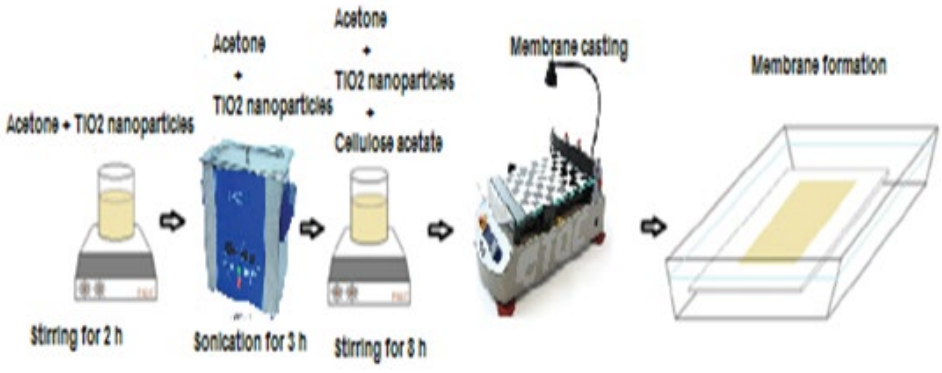

Fig. 2. Membrane formation process.

110–120 μm. In the method described in this manuscript, the nonwoven fabric is pasted to the glass plate to prevent the bleeding of polymer solution which leads to the formation of air pockets.

2.4. Experimental setups and operating conditions

In order to obtain trustworthy and accurate experimental results, the laboratory-scale test systems must be well designed and fabricated to simulate as closely as a possible actual full-scale system with minimal differences. The main experimental setups used in this paper comprised of the laboratory-scale FO system and the laboratory-scale NF (suitable for RO as well) system. The detailed description of each system is given.

2.4.1. Laboratory-scale FO system

Fig. 3 shows the schematic diagram of the laboratory-scale FO system while Fig. 4 shows the schematic diagram of the hybrid FO-NF system configuration.

The laboratory-scale FO system included a specially designed cross flow membrane cell which has a symmetric channel on each side of the membrane. These Sterlitech CF042 clear cast acrylic FO membrane cells are laboratory-scale, modified forward osmosis filtration units designed

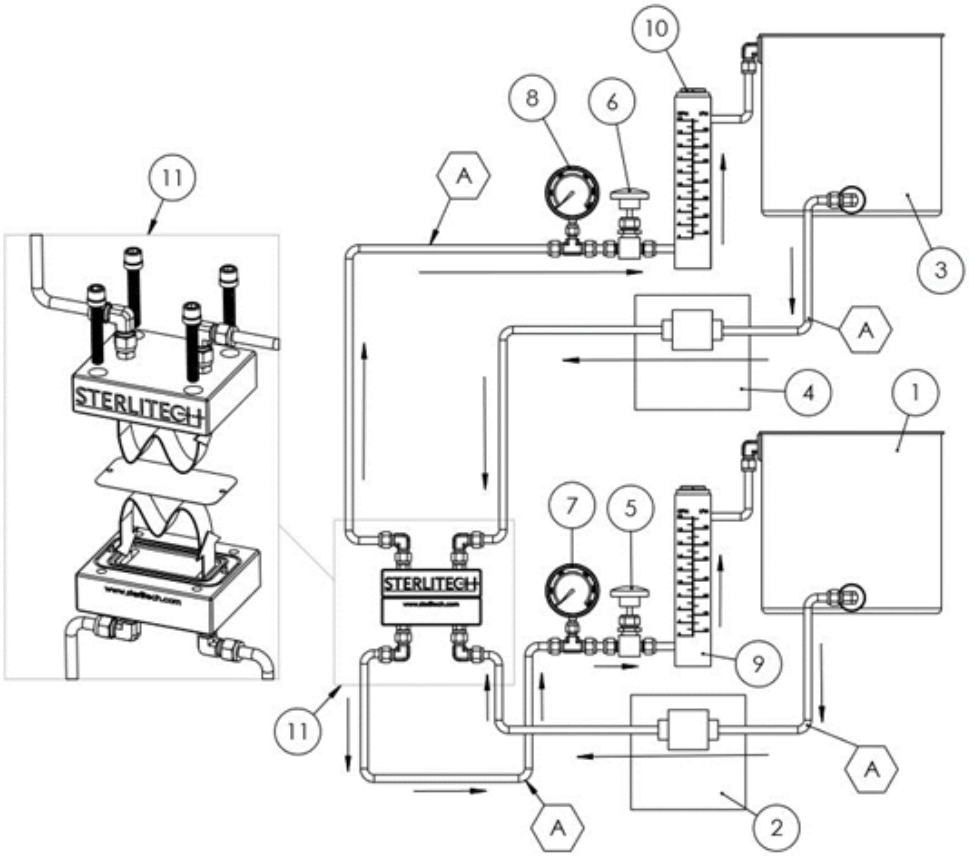

CF042SS/ CF042HAS/ CF042A FO Flow Diagram	
Item No.	Part Description
1	Feed Tank
2	Feed Pump
3	Draw Solution Tank
4	Draw Solution Pump
5	Concentrate Pressure Control Valve
6	Draw Solution Pressure Control Valve
7	Concentrate Pressure Gauge
8	Draw Solution Pressure Gauge
9	Concentrate Flow Meter
10	Draw Solution Flow Meter
11	CF042-FO Cell Assembly
A	3/8" Low Pressure Tubing

STERLITECH Corporation
www.sterlitech.com sales@sterlitech.com

Fig. 3. Schematic diagram of the lab scale forward osmosis experimental set up with NaCl feed and $MgSO_4$ draw solution.

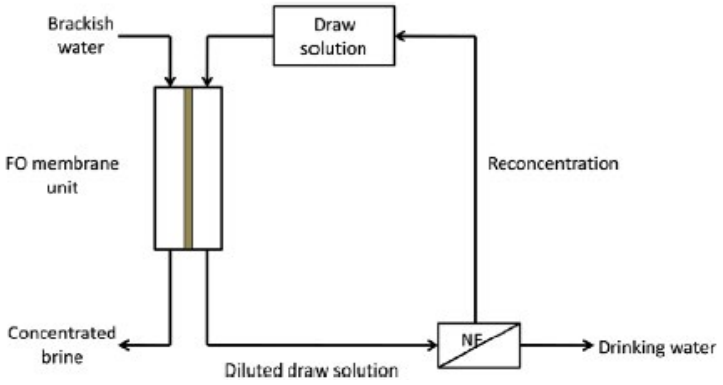

Fig. 4. Schematic diagram of the hybrid FO-NF system configuration.

to provide fast and accurate performance data with minimal amounts of product, expense, and time. The outer dimensions were 12.7 cm × 10 cm × 8.3 cm (5 in × 4 in × 3.25 in) for cell length, width, and height, respectively. Active area dimensions are 9.207 cm × 4.572 cm (3.625 in × 1.8 in).

This cell made from acrylic and has maximum pressure 27.6 bar (400 psig), active membrane area 42 cm^2 (6.5 in^2) and maximum temperature of 80°C. The draw and feed solutions flowed on the permeate side and co-currently on the feed side, respectively, both of which were controlled independently by a KNF pump remote controlled for feed solution, its flow rate 0.2–1.3 L min^{-1} and has maximum pressure 90 psi (Sterlitech cooperation, USA) and peristaltic variable flow pump for draw solution, its flow rate 10–600 mL min^{-1}, the cross flow rates were measured with a flow-meter (Blue-white Industries Ltd., model no. F-55375L, USA). The volumetric flow rates for the experiments were 0.8 L/min and 0.4 L min^{-1} for feed and draw solution, respectively. A weighing scale (SB16001, Mettler Toledo, Germany) was used to monitor the weight changes of the feed solution due to the water flux across the membrane, from which the water flux was calculated. Two stainless steel tanks its capacity is 9 L were used, one for the feed solution and the other for the draw solution.

In this paper, since the unit was operated by recycling the feed and draw solutions, the water flux would decrease significantly with time as the draw and feed solution would be diluted and concentrated with time, respectively. Hence, the initial water fluxes of the operation, which was calculated from the first 90 min of the experimental run. Prior to starting of each experimental run, the air was purged from both the flow channels, and the fluid flows in both the channels were allowed to be stabilized for 5 min. This was necessary to facilitate the development of both external concentration polarization and ICP layer and to ensure that the fluid flow rates were stabilized.

2.4.2. Laboratory-scale nanofiltration system

The nanofiltration (NF) experiments were conducted using a PurePro nanofiltration (NF) membrane model number NF33-1812-80. Nanofiltration membrane has a slightly larger pore size than reverse osmosis membrane. Thus, monovalent salts like sodium chloride (common table salt) molecules pass through the membrane but larger divalent salts of calcium, magnesium, and other metals like iron, heavy metals, etc. are all blocked. NF membrane capacity is 80 GPD. The feed water (diluted draw solution) that was stored in a stainless steel cylindrical tank was circulated into the membrane cell by a KNF pump. NF membrane specification and operation limits see Table 1. Fresh NF membrane was compacted for 2 h at 600 psi prior to each experiment.

2.4.3. Sampling methods

In the conductivities measurements, the conductivity probe was directly immersed into the feed solution tank, draw solution tank, and permeate tank for conductivity measurement. Samplings of liquid samples were carried out for other analyses. Draw, feed solutions, and NF permeate samples were collected from their respective tanks. If the samples were not immediately used for analysis, the samples were stored at 4°C for at most 1 d.

2.5. Characterizations of nanoparticles and membranes

2.5.1. Scanning electron microscopy

Surface images of nanoparticles and membrane's surface were recorded using Quanta FEG 250 scanning electron microscopy (SEM; FEI Company, Hillsboro, Oregon-USA) at Egyptian Desalination Research Center of Excellence (EDRC), Desert Research Center (DRC), Cairo. Samples were mounted onto SEM stubs. Applied SEM conditions were: a 10.1 mm working distance, with an in-lens detector with an excitation voltage of 5 kV for membranes and 20 kV for ZnO NPs. The membranes were snapped under liquid nitrogen to give a generally consistent and clean cut. Cross-sectional images of the membranes were obtained also.

2.5.2. X-ray diffraction

The X-ray diffraction patterns of films and nanoparticles were measured with ARL™ X'TRA powder diffractometer (Thermo Fisher Scientific Inc., USA) at Science and Technology Center of Excellence (STCE), Cairo. The diffraction patterns were recorded using metal ceramic tube Cupper (with Cu-K-alpha wavelength = 1.5405981 Å

Table 1
NF membrane specification and operating limits

Material	
Membrane	Polyamide composited (from the USA)
Backing material	Polyester
Permeate carrier	Tricot
Feed spacer	PE
Collective tube	ABS
Glue	Polyurethane
O-ring	EPDM
External Warp	Opp tape
Operation limits	
Membrane type	Polyamide thin film composite
Maximum operating pressure	600 psig (40.0 bar)
Maximum pressure drop	13 psi (0.9 bar)
Maximum operating temperature	113°F (45°C)
pH range	2–11
Maximum feed water turbidity	1 NTU
Maximum feed flow rate	2 GPM (7.6 LPM)
Free chlorine tolerance	<0.1 ppm

target with scintillation detector (NaI (TI) scintillation crystal) at current 44 mA and voltage 45 KV. The data compared to the International Centre for Diffraction Data [27].

2.5.3. Contact angle measurement

The hydrophilicity of the membrane surface was measured using a drop shape analyzer–DSA25 (Krűss, Germany) at EDRC, DRC, Cairo, used the sessile drop method at 25°C. A water drop was placed onto the membrane surface with a digital micro-syringe with a contact angle between the water and the membrane measured when no further change was observed. On average, eight measurements were obtained for each membrane sample.

2.5.4. Mechanical properties

The mechanical properties of the membrane samples were measured with TA Instruments Q-Series DMA (Q800) at EDRC, DRC, Cairo, where the dynamic strain and stress were measured at room temperature (25°C). Tensile tests were carried out to assess Young's modulus and strain at fracture of samples at the rate of 10 mm min^{-1}. The membrane samples were cut into rectangles with a dimension of 17 mm × 12 mm × 0.10 mm, and fixed perpendicular to one another in between two automatic gripping units of the sample, leaving a 3 cm sample extent for mechanical loading. The thickness of the membrane samples was determined with an automatic micrometer with a precision of 1 μm. Young's modulus (Mega pascal, Mpa) was calculated using the following equation:

$$\text{Young's modulus}(\text{Mpa}) = \frac{\text{Stress}}{\text{Strain}} \quad (1)$$

2.5.5. Attenuated total reflectance–Fourier transform infrared spectroscopy

Analysis by Infrared spectroscopy was carried out using Nicolet iS50 attenuated total reflectance–Fourier transform infrared spectroscopy (ATR–FTIR) spectrophotometer at EDRC, DRC, Cairo.

2.5.6. Surface area and pore size analyzer

Surface area and pore size of CA and CA modified with ZnO NPs membranes were measured using BELSORP measuring instruments (BELSORP mini-II, Japan, Inc.) at National Institute of Oceanography and Fisheries–NIOF. The specific surface area (SSA) was calculated using the Brunauer–Emmett–Teller (BET) equation.

2.5.7. Testing of membranes in forward osmosis process

The feed solution was prepared by dissolving sodium chloride in 4 L of distilled water (TDS = 1,000 ppm). The draw solution was prepared by dissolving anhydrous magnesium sulphate in 4 L of distilled water (TDS = 10,000 ppm). Feed solution reservoirs were placed on weighing balances and were circulated at a rate of 0.8 and 0.4 L min^{-1} for feed and draw solutions, respectively in a closed loop using gear pumps. All the experiments were conducted at 25°C with a feed solution on the active side of the membrane. The area of the membrane used in the FO runs is 0.0042 m^2.

2.5.8. Determination of water flux and salt rejection

The amount of water permeated over a period of time, flux (L h^{-1} m^{-2}) was measured from the change in the weight of feed solution during FO run. Salt rejections were calculated by measuring the Na and Mg concentrations in the feed and draw solution before and after FO runs by using the Eq. (2):

$$J_w = \frac{\Delta\text{Volume}}{\text{Water density} \times \text{Membrane surface area} \times \text{time}} \quad (2)$$

$$R\% = \left[1 - \frac{C_p}{C_r}\right] \times 100 \quad (3)$$

where J_w is water flux, C_p is the concentration of the Na or Mg in the draw and feed solutions, respectively after the FO run and C_r is the concentration of the Na or Mg in the feed and draw solutions, respectively at the beginning of the experiment [28]. Feed and draw solution samples before and after FO runs were analyzed using inductively coupled plasma mass spectrometry (ICP–MS) for determining the concentration of Mg, flame photometer for determining the concentration of Na, and Ion chromatography (Dionex, ICS-1100, Thermo Fisher Scientific, USA) for determining the concentration of Cl.

3. Results and discussions

3.1. Characterization of the synthesized ZnO NPs

3.1.1. X-ray diffraction

The X-ray diffraction (XRD) spectrogram of ZnO nano-particles synthesized using zinc chloride with water medium is shown in Fig. 5. In Fig. 5 the distinctive ZnO peaks at 32.90, 34.5, 36.40, 47.62, 57.28, 63.78, 72.88, and 77.2, respectively. Fig. 5 exhibits peaks similar to those reported for ZnO which suggests the formation of ZnO nanoparticles [29]. The XRD pattern for ZnO nanoparticles obtained with water medium shows much sharper peaks. This means that the crystallinity is more for ZnO nanoparticles. The peak at 11.52 is for SLS surfactant indicates that some impurities of SLS found in ZnO NPs.

3.1.2. Scanning electron microscopy

The surface morphology of ZnO NPs was characterized by SEM. In Fig. 6, the ZnO nanoparticles appear in sphere shapes with smooth surfaces.

3.2. Effect of polymer concentration on membrane performance

The objective of this section is to study the effect of polymer concentration on membrane performance in the FO process. Therefore, membranes were fabricated at different polymer concentrations for a fixed solvent system. The prepared membranes were then tested in the FO process and evaluated in terms of water flux and salt rejection (Table 2). Finally, SEM pictures of the prepared membranes were recorded to observe their morphology.

Membranes with polymer concentrations varying from 4 to 10 wt.% CA were cast using only acetone. The fabricated membranes were tested in the FO process and the results will be presented and discussed below (Fig. 7). As can be observed, increasing CA concentration from 7% to 10% intensifies the thermodynamic instability of the cast film solution and thus demixing of this concentrated solution can be performed with less amount of nonsolvent. Also, increase in the CA concentration from 7% to 10% results in a noticeable increase in viscosity values and this result in an intensive reduction of mutual diffusivities between the non-solvent (water) and the solvent (acetone) in the system during solidification of the casting solution. Thus, using higher values of CA, the precipitation process is stopped after a longer time and this leads to preparation of thinner and dense membranes. Both porosity and thickness of the synthesized membrane were reduced by increasing CA concentration [30]. Increasing polymer concentration in the casting solution results in a more concentrated interface casting solution/non-solvent during phase inversion, which slows down the solvent/non-solvent exchange leading to delayed demixing. Therefore, the resulting membranes display denser skin-layers and sub-layers [31].

Finally, it was found out that increasing CA concentration in the casting solution slowed down the demixing process. The delayed demixing prevented the immediate growth of nuclei in the membrane structure. This resulted in the creation and distribution of a large number of small nuclei throughout the cast film and consequently the formation of a denser structure. Pure water permeation flux was directly related to the number of pores and their size in the membrane top layer. It can be said that the rising concentration of CA up to a "certain value" increases the porosity of the synthesized membranes. Further concentrations lead to suppression of macrovoids and formation of denser structures in the sub-layer so water flux decrease [32].

3.3. Effect of thickness on membrane performance

To study the influence of the thickness of the liquid film in the performance of the membranes, we fabricated membranes with 50, 100, and 200 μm. Note that the indicated thickness is the thickness of the calibrated ruler, not the final membrane thickness since this is the control parameter, however, we will present the results for water flux and salt rejection for the initial liquid film thickness of the membrane. The membranes were produced using the same solution and under the effect of similar external conditions (mainly temperature and humidity), the only changes being the ruler (for obtaining a different thickness of the liquid film) and the consequent preparation parameters.

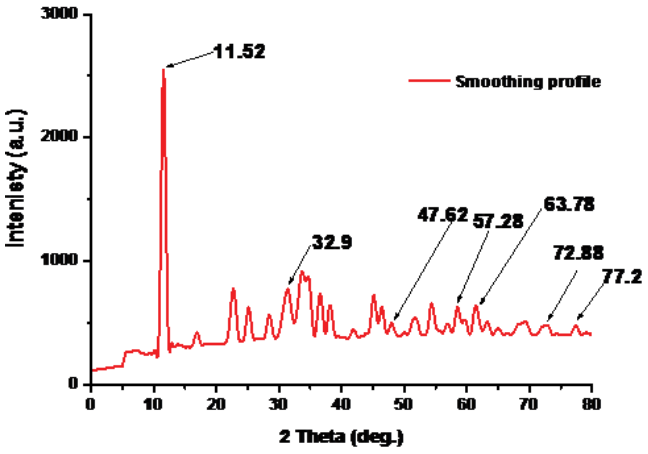

Fig. 5. XRD pattern of ZnO nanocrystal.

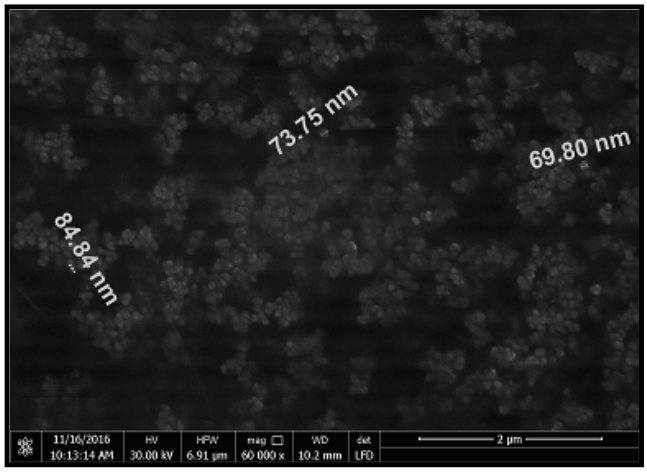

Fig. 6. SEM micrographs of ZnO NPs.

Table 2
Effect of polymer concentration on water flux and salt rejection

Membrane code	Component compositions		Flux ($L\ h^{-1}\ m^{-2}$)	*R*% Mg	*R*% Na	*R*% Cl
	CA (wt.%)	Acetone (wt.%)				
M1	4	96	6.33	93.5	92.4	92.4
M2	6	94	7.52	98.5	97.6	97.5
M3	7	93	9.9	99.95	98.8	100
M4	8.5	91.5	8.71	99.96	99.4	100
M5	10	90	7.52	99.97	100	100

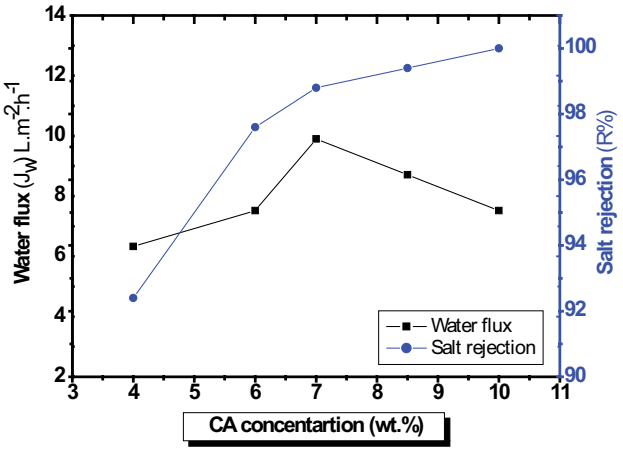

Fig. 7. Effect of CA concentration on water flux and salt rejection (1,000 ppm NaCl as feed concentration and 10,000 ppm $MgSO_4$ as draw concentration, flow rate 0.8 and 0.4 L min^{-1} for feed and draw solutions, respectively. All the experiments were conducted at 25°C with a feed solution on the active side of the membrane. The area of the membrane used in the FO runs is 0.0042 m^2).

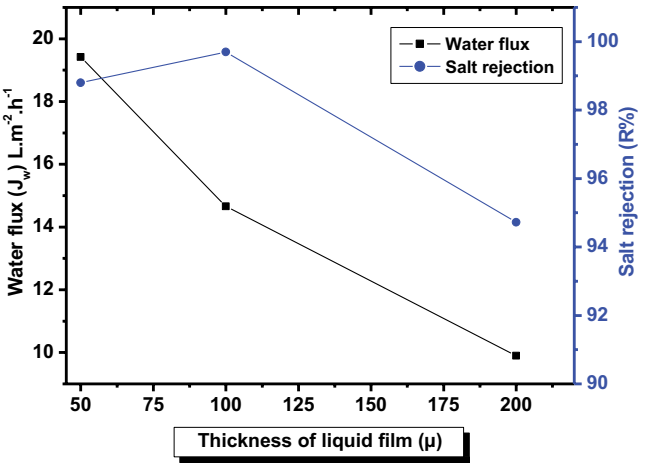

Fig. 8. Effect of thickness of a liquid film on water flux and salt rejection (operation conditions as mentioned above in Fig. 7).

The average value of the water flux (J_w), and salt rejection (*R*%) for three membranes obtained are presented in the following Table 3. Fig. 8 presents the results of water flux and salt rejection for the membranes produced with a different thickness of the initial liquid film. Our result showed that water flux of membranes is indirectly proportional to their thickness. On the contrary, the salt rejection increases slightly with membrane thickness.

Concerning the *R*% values, it was proved that it increases with the thickness of the initial liquid film, for the lower thicknesses, obtaining a similar value for the higher thicknesses evaluated.

The selective layer is formed in a smooth way when the thickness is higher and this is probably the cause for the observed behavior, which means that the optimum value of the thickness is therefore 50 μm, which corresponds to a final thickness of the membrane of 20 μm. Previous studies [33–35] showed that water flux of membranes is indirectly proportional to their thickness. Conversely, the salt rejection increases slightly with membrane thickness depending mostly on the coherence of the dense film [36]. Considering the results, and as expected, J_w values decrease with the thickness of the initial liquid film increases this is due to the overall pressure drops across the membrane microporosity (selective layer).

3.4. Membrane modification by incorporation of ZnO nanoparticles

ZnO NPs have been used for modifications of CA–FO membrane resulting in a ZnO NPs modified CA membrane.

Table 3
Effect of different thickness of a liquid film on membrane water flux and salt rejection

Membrane code	Preparation variables		Flux ($L\ h^{-1}\ m^{-2}$)	*R*% Mg	*R*% Na	*R*% Cl
	CA (wt.%)	Thickness (μ)				
M6	7	50	19.42	99.95	98.8	100
M7	7	100	14.66	99.97	99.7	100
M8	7	200	9.9	99.7	94.72	100

Using the synthesized ZnO NPs in CA membrane lead to enhance the hydrophilicity, increase the roughness, surface area and increase the interaction sites for more binding of ZnO NPs on the membrane surface [37]. So, this modification not only increases the functional groups on the membrane surface but also decreases the space hindrance for attracting ZnO NPs.

The relationship of the water flux and salt rejection of the membranes against the ZnO NPs amount is presented in Fig. 9. The performance of the membranes with different contents of ZnO NPs has been investigated in terms of water flux and salt rejection as shown in Table 4. The water flux and salt rejection for the CA and modified CA with ZnO NPs concentrations ranging from 0.005 to 0.5 wt.%. The ZnO NPs modified CA membranes showed superior water flux and salt rejection than the pure CA membrane. An optimum membrane performance was obtained at 0.25 wt.% of the ZnO NPs. The water flux was 26.57 L h^{-1} m^{-2}, while the salt rejection was 99.5%. The higher water flux and the salt rejection of these membranes may be explained by the presence of the polar surface of the ZnO NPs. This surface is rich in hydroxyl (OH) groups and helps to adsorb ions during the desalination process. At a low loading amount of ZnO NPs (0.1–0.25 wt.%), a structure with higher porosity is formed on the top surface of CA and it enhanced the water flux all over the membrane, this is attributed to the presence of active hydrophilic functional groups on the membrane surfaces [38]. The improvement of salt rejection with loading ZnO NPs (0.05–0.1 wt.%), this may be due to the dense surface caused by the good interaction of ZnO NPs with the CA matrix membrane.

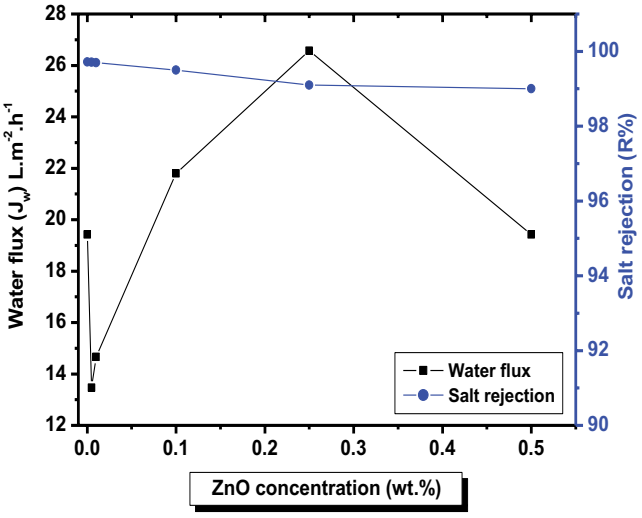

Fig. 9. Effect of ZnO NPs concentration on water flux and salt rejection (operation conditions as mentioned above in Fig. 7).

SEM was used to observe the surface and cross-sectional morphology of each membrane, including CA and ZnO NPs modified CA membrane. Figs. 10a and c show the CA with a smooth surface. Figs. 10b and d show the surface of ZnO NPs modified CA, where a dense structure was observed. The modified ZnO NPs membrane shows nodules, and the pore size was found to increase with an increase in ZnO NPs concentration. Additional ZnO NPs in the dope solution lead to rougher membrane surfaces. It is apparent that the ZnO NPs are uniformly dispersed along the membrane surface, which exhibits increased pore density and pore size.

It is believed that the addition of ZnO NPs make efficient the membranes surface properties and generates new flow paths through the membrane layer, causing an increase in water sorption and permeability.

Cross-sectional inspection of the membranes was also made under SEM (Figs. 11a and b). The cross sections of the CA layer before ZnO NPs modification show a spongy structure.

A homogeneous propagation of the nanoparticles in the polymer matrix is shown on the surface, and there is little evidence of ZnO NPs agglomerations near the surface of the CA membrane. ZnO NPs modified CA membrane show smooth, homogeneous surfaces, and seemingly large porosity with less porous voids near the surface. These enhancements in the membrane surface lead to new flow paths in the membrane layer allowing increased water flux and sorption.

Hence, ZnO NPs constructed a membrane with the tightly packed surface and spongy structure with a very thin skin layer, explaining the high solutes rejection rates [39].

3.5. Characterization of the synthetic forward osmosis membranes

The membranes were characterized by ATR–FTIR spectroscopy, X-ray diffraction, mechanical properties, and the change in morphology by SEM, the contact angle, and surface area and pore size, as follows.

Table 4
Effect of different concentration of ZnO NPs on membrane water flux and salt rejection

Membrane code	Dope compositions		Flux (L h^{-1} m^{-2})	*R*% Mg	*R*% Na	*R*% Cl
	CA (wt.%)	ZnO (wt.%)				
M9	7	0	19.42	99.7	99.12	100
M10	7	0.005	13.47	99.7	99.10	100
M11	7	0.01	14.66	97.7	99.7	100
M12	7	0.10	21.8	99.9	99.5	100
M13	7	0.25	26.57	99.6	99.5	100
M14	7	0.50	19.42	99.3	99	100

3.5.1. Attenuated total reflectance–Fourier transform infrared spectroscopy

Spectroscopic analysis plays an important role in the polymeric membrane characterization in order to investigate the incorporated components of the membranes. ATR–FTIR spectrums of CA and CA-modified membranes are given in Fig. 12. In case of control, peak at 3,479 cm^{-1} represented stretching of O–H, it indicates the presence of hydrogen bonding between hydroxyl group in the cellulose network and also the surface OH groups, 1,735 cm^{-1} depicted the strong peak for C=O of carbonyls, 1,431 cm^{-1} indicated bending of C–H followed by peaks at 1,367 and 1,215 cm^{-1} rocking and wagging mode of C–H bond. The strongest peak at 1,035 cm^{-1} specified C–O–C while the peak at 1,160 and 901 cm^{-1} illustrated the presence of saccharide. Similar results had been previously reported in the literature [40,41]. The band at 901 cm^{-1} (cellulose II) was assigned to C–O–C stretching at β-linked glucose of cellulose [42,43]. A similar observation was also found in the previous study [44]. In Fig. 12 peaks at 2,915 cm^{-1} correspond to the asymmetric C–H stretching, 1,735 cm^{-1} corresponds

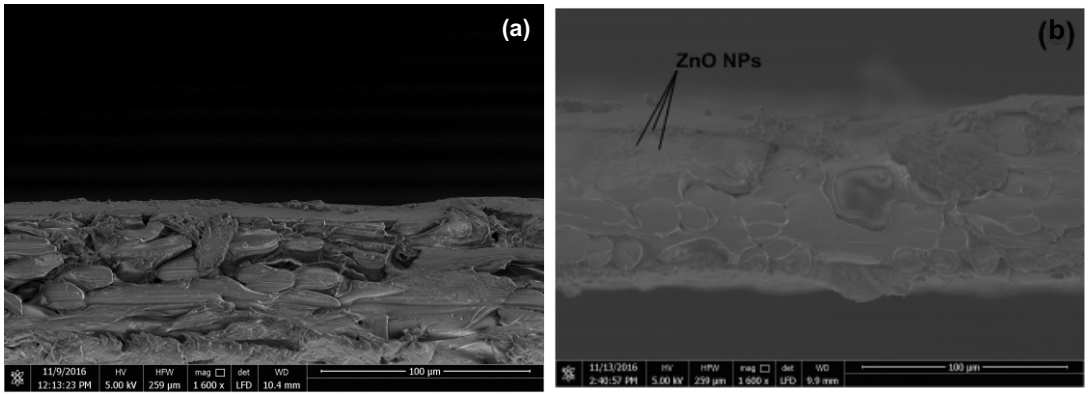

Fig. 11. SEM micrographs of CA membranes (50 μm) with ZnO NPs. Cross section (1600×) (a) pure CA and (b) 0.25 wt.% ZnO.

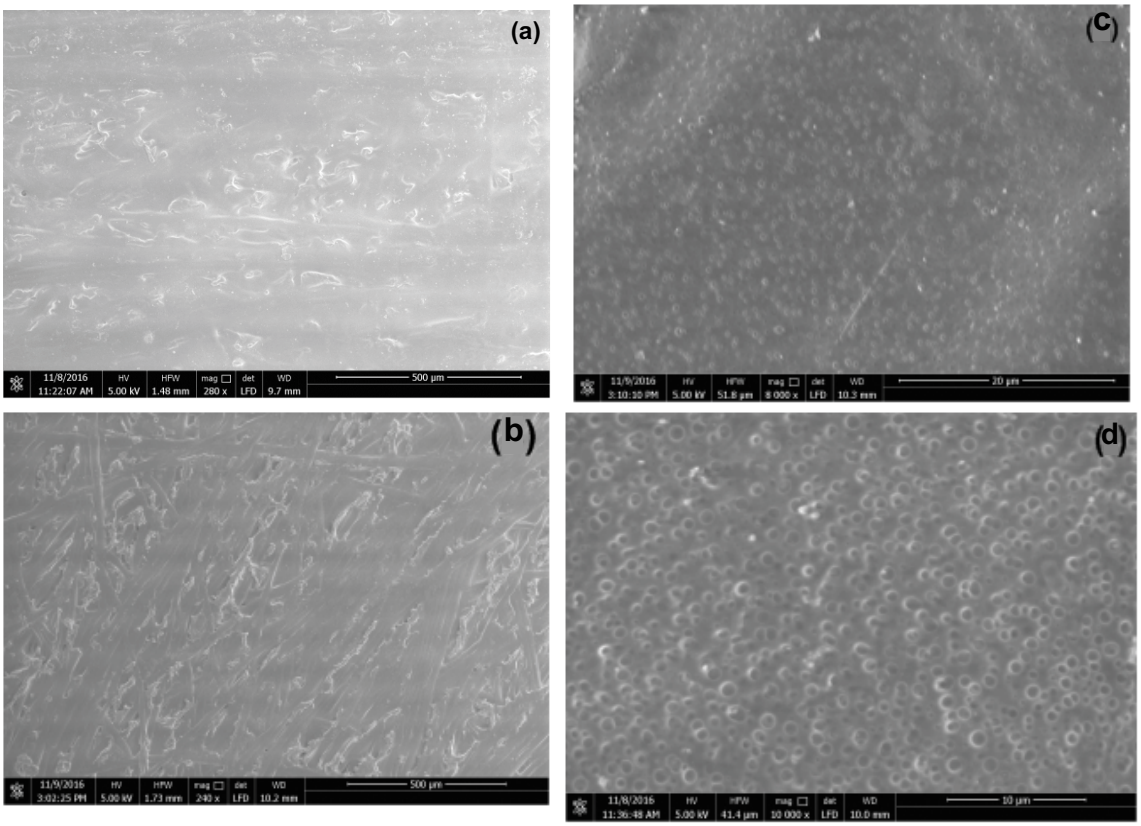

Fig. 10. SEM micrographs of CA membranes (50 μm) with different types of nanomaterials. Top surface (260×) (a) pure CA, (b) 0.25 wt.% ZnO, top surface (8000×), (c) pure CA, and (d) 0.25 wt.% ZnO (10000x).

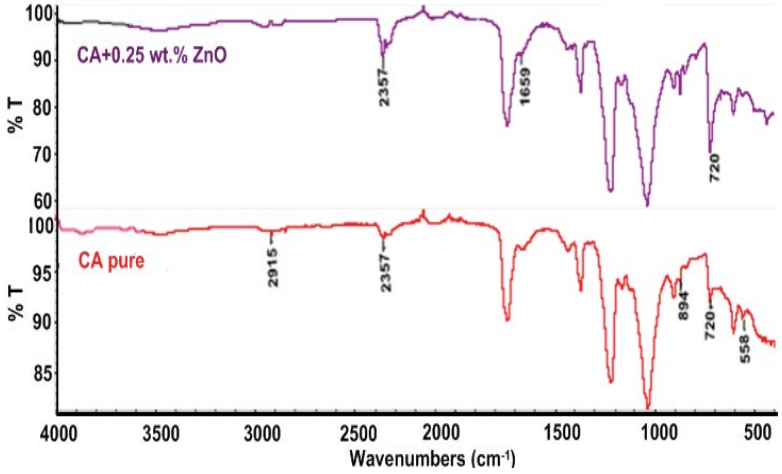

Fig. 12. ATR–FTIR spectra of CA and CA modified with 0.25 wt.% ZnO NPs membranes.

to C=O stretching, 1,160 cm^{-1} (asymmetric stretching of the C–O–C bridge) and 1,215 cm^{-1} (carboxylate C–O stretch) is also observed [45]. These peaks were also observed for the hybrid membrane.

The spectrum of the ZnO NPs modified CA membrane is shown in Fig. 12. Comparing the ZnO NPs CA membrane with the pure CA membrane illustrates that there is a stretching vibration band that appears at approximately 1,659 cm^{-1}. This band is most largely caused by COO–Zn, representing the covalent bond between the –COOH group of the CA and the hydroxyl (–OH) group on the surface of the ZnO NPs [46]. The appearance of the hydroxyl (–OH) group peak around 3,480 cm^{-1}, is due to the formation of the intramolecular hydrogen bond between the carboxylic groups (COO–) of CA and the hydroxyl group on the surface of the ZnO NPs [47]. The CA is flexible, and the hydroxyl groups on the surface of the ZnO NPs can easily find a carbonyl group to form the hydrogen bond that will be stabilized on the membrane surface. The integration of ZnO NPs into the CA solution is inferred by the shift of the carboxylic peak due to electron acceptance from the Zn atoms [48]. This shift is due to the interaction between the carboxylic groups (COO–) contained in the CA and the ZnO NPs [49]. Finally, these peaks indicate the successful integration of ZnO NPs in CA membrane [50].

3.5.2. X-ray diffraction patterns

The degree of crystallinity of CA membranes was evaluated qualitatively using X-ray diffraction by determination of the area of the scattering peaks presented in Fig. 13. The XRD diffraction patterns of X-ray diffraction patterns of CA/ZnO hybrid membrane (with 0.25 wt.% ZnO) and CA membrane are shown in Fig. 13.

It can be observed that the pattern of CA membrane has four crystalline characteristic peaks at 2θ of 14.16°, 17.04°, 18.00°, 22.92°, and 26.28° corresponding to cellulose I as pdf card no. 00-003-0226 according to International Centre for Diffraction Data (2017). The peaks corresponding to ZnO did not appear due to a very small amount of ZnO NPs (0.25 wt.% from CA concentration) present in CA matrix [51].

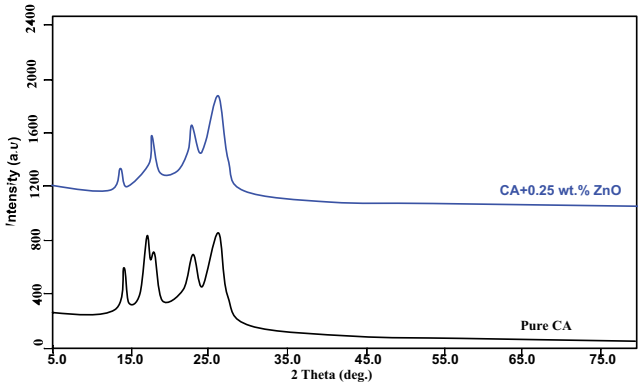

Fig. 13. X-ray diffraction patterns of CA/ZnO (with 0.25 wt.% ZnO) and pure CA membrane.

In the case of ZnO NPs peaks at 17.04 and 18.00 appear as one peak at 18.04 and peaks shifted to higher angles compared with those of CA that also indicate that ZnO interacts with CA. It is observed that crystallinity decrease in case of make modification to CA with ZnO NPs as shown in Table 5.

3.5.3. Mechanical properties of the synthetic membranes

The mechanical properties of CA and CA/ZnO NPs membranes are shown in Table 6 and the stress-strain curves are shown in Figs. 14 and 15. The CA modified ZnO NP membranes show decreasing in tensile strength (Mpa), and improvement in elongation break.

The mechanical properties of the ZnO NP modified CA has been enhanced by the addition of a small amount (0.25 wt.%) of ZnO NPs onto the membrane, causing increased elongation. The mechanical properties of the membrane depend mainly on the membrane microstructure and intermolecular forces operating along the membrane backbone [52].

The addition of small amounts of ZnO NPs to the membrane surface causes a uniform dispersal of ZnO NPs in the

Table 5
Crystallinity of control and CA modified membranes

Sample	Crystallinity (%)
Pure CA	59.57
CA + 0.25 wt.% ZnO	50.46

Table 6
Tensile stress and elongation-at-break of control and modified membrane (50 μm thickness)

Membrane type	Tensile stress (MPa)	Elongation (%)	Young's modulus (MPa)
Pure CA	16.17	1.74	266.2
0.25 wt.% ZnO	15.13	13.27	312

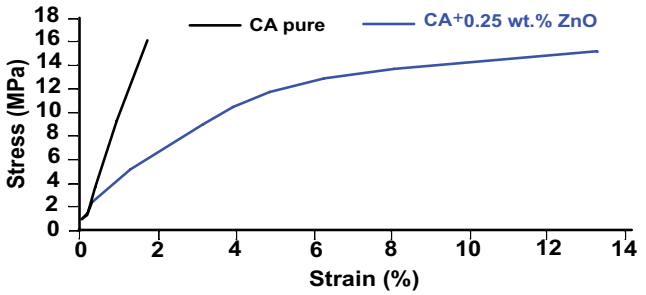

Fig. 14. Mechanical properties of pure CA and CA modified with 0.25 wt.% ZnO NPs membranes.

membrane matrix. This dispersal provides higher uniform stress distribution, the reduced creation of stress-concentration centers, and consequently enhances the elongation properties of the membrane [53].

3.5.4. Hydrophilicity of the membranes

The contact angle is an important parameter for measuring surface hydrophilicity. In general, a smaller contact angle corresponds to a more hydrophilic material. It is evident from Fig. 16 that there is a decrease in contact angle by adding ZnO NPs concentrations as shown in Table 7. These results demonstrated that additives can improve the hydrophilicity of the membrane. The less hydrophilic surface shows a larger contact angle with the surface and vice versa.

At first, it should be noted that water flux depends on both membrane porosity and also membrane hydrophilicity [54,55]. Thus, the mentioned reduction of water flux cannot be related to the membrane porosity and thus only can be related to the membrane hydrophilicity. According to Fig. 16, adding ZnO NPs results in a lower contact angle and consequently higher membrane hydrophilicity.

The ZnO NPs modified CA membrane show a lower contact angle of approximately 47.6 ± 2° at room temperature, suggesting that the surface hydrophilicity increased with surface modifications. The improved hydrophilicity of the ZnO NPs modified CA membrane may be due to a

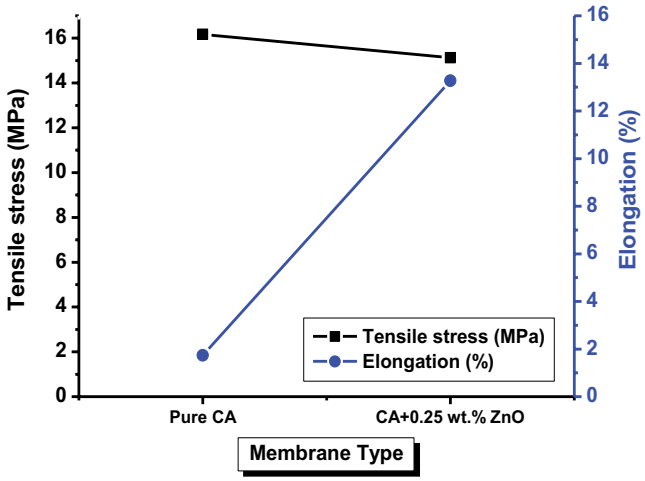

Fig. 15. Tensile stress and elongation-at-break of control and modified membrane (50 μm thickness).

Table 7
Contact angle of control and modified membranes

Membrane type	Contact angle θ (°)
Pure CA	63.85 ± 2
0.25 wt.% ZnO	47.6 ± 2

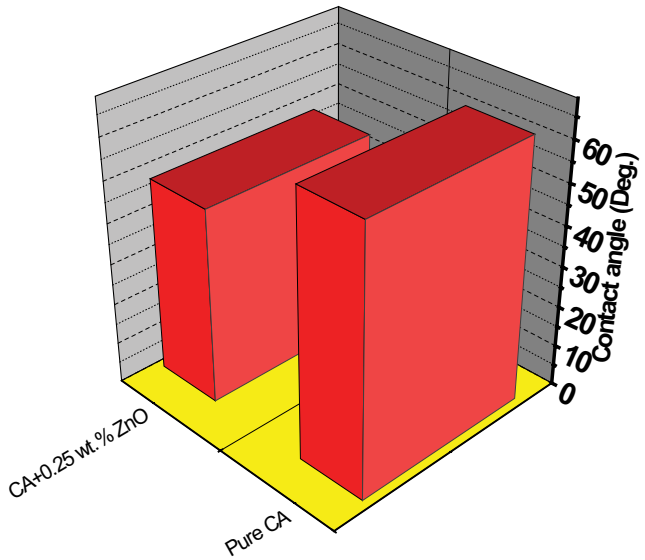

Fig. 16. Contact angle of control and modified membrane.

greater attraction of water molecules by the nanoparticles, and to the presence of active hydrophilic functional groups on the membranes surfaces. The contact angle decreased upon addition of the ZnO NPs causing an increase in the surface energy. This increase in surface energy allows water to easily spread onto the surface and increases the capability of the hydrophilic pores to imbibe water via capillary effects [56].

3.5.5. Surface area and pore size

BET analysis provides precise SSA evaluation of membranes by nitrogen multilayer adsorption measured as a function of relative pressure using a fully automated analyzer. The technique encompasses external area and pore area evaluations to determine the total SSA in m^2 g m^2 g^{-1} yielding important information in studying the effects of surface porosity and pore size. It is evident from Fig. 17 that there is an increase in surface area and total pore volume by adding ZnO NPs. These results demonstrated that additives can improve the surface area and porosity of the membrane.

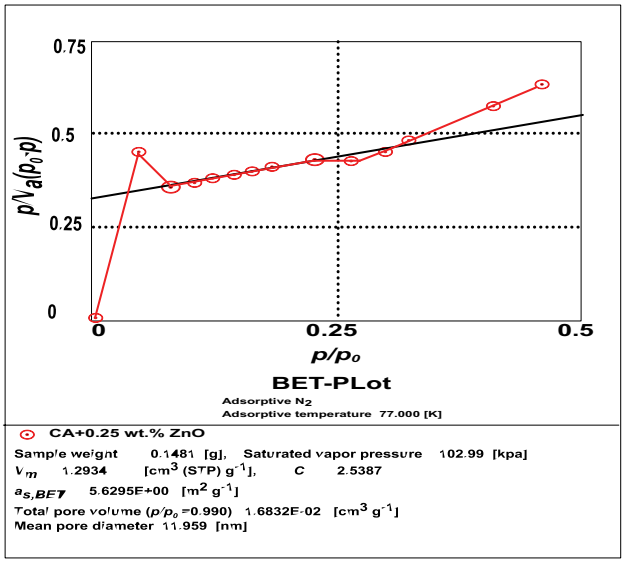

Fig. 17. Specific surface area, mean pore diameter, and total pore volume of CA modified with 0.25 wt.% ZnO NPs.

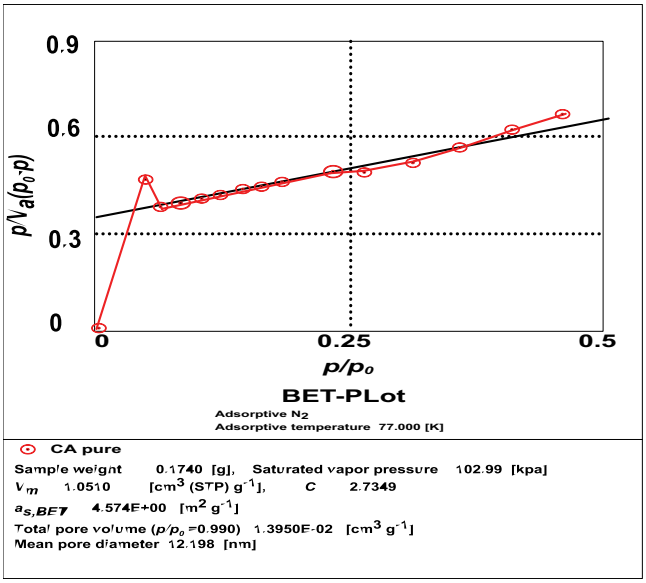

Fig. 18. Specific surface area, mean pore diameter, and total pore volume of control membrane.

The ZnO NPs modified CA membrane show a high surface area and total pore volume of approximately 5.63 m^2 g^{-1} and 1.68×10^{-2} cm^{-3} g^{-1}, respectively. For pure CA membrane, the surface area and total pore volume were 4.57 m^2 g^{-1} and 1.39×10^{-2} cm^{-3} g^{-1}, respectively (Figs. 17 and 18). The water flux increase in case of CA modified with ZnO NPs is due to increasing in surface area and total pore volume than the control by 23% and 20%, respectively.

4. Conclusion

A reliable method for the bench scale casting of FO membranes was developed and successfully applied to cast CA membranes. CA/ZnO membrane was synthesized using the phase inversion method. The effect of polymer concentration, membrane thickness, and ZnO NPs on water flux and salts rejection in the FO process were investigated. Membranes prepared with ZnO gave high flux and salt rejection 99.5% of Na^+, 100% of Cl^- and 99.6% of Mg^{+2} in FO runs. The water flux increase in case of CA modified with ZnO NPs is due to increasing in surface area and total pore volume than the control by 23% and 20%, respectively, and also ZnO NPs improve the hydrophilicity of the membrane. This proves that the CA/ZnO membrane can improve the membrane performances.

Acknowledgment

The authors wish to acknowledge the financial support Egyptian Egyptian Water Desalination Alliance funded Academy of Scientific Research and Technology, Egypt.

References

[1] A. Tiraferri, N.Y. Yip, W.A. Phillip, J.D. Schiffman, M. Elimelech, Relating performance of thin-film composite forward osmosis membranes to support layer formation and structure, J. Membr. Sci., 367 (2011) 340–352.
[2] R.W. Holloway, T.Y. Cath, K.E. Dennett, A.E. Childress, Forward Osmosis for Concentration of Anaerobic Digester Concentrate, Proceedings of the AWWA Membrane Technology Conference and Exposition, Phoenix, AZ, 2005.
[3] A.M. Awad, R. Jalab, J. Minier-Matar, S. Adham, M.S. Nasser, S.J. Judd, The status of forward osmosis technology implementation, Desalination, 461 (2019) 10–21.
[4] T.Y. Cath, A.E. Childress, M. Elimelech, Forward osmosis: principles, applications, and recent developments, J. Membr. Sci., 281 (2006) 70–87.
[5] S. Zhang, K.Y. Wang, T.-S. Chung, Y. Jean, H. Chen, Molecular design of the cellulose ester-based forward osmosis membranes for desalination, Chem. Eng. Sci., 66 (2011) 2008–2018.
[6] R.C. Ong, T.-S. Chung, B.J. Helmer, J.S. de Wit, Novel cellulose esters for forward osmosis membranes, Ind. Eng. Chem. Res., 51 (2012) 16135–16145.
[7] G. Han, T.-S. Chung, M. Toriida, S. Tamai, Thin-film composite forward osmosis membranes with novel hydrophilic supports for desalination, J. Membr. Sci., 423 (2012) 543–555.
[8] K.Y. Wang, T.S. Chung, G. Amy, Developing thin-film composite forward osmosis membranes on the PES/SPSf substrate through interfacial polymerization, AICHE J., 58 (2012) 770–781.
[9] C. Qiu, S. Qi, C.Y. Tang, Synthesis of high flux forward osmosis membranes by chemically crosslinked layer-by-layer polyelectrolytes, J. Membr. Sci., 381 (2011) 74–80.
[10] Q. Saren, C.Q. Qiu, C.Y. Tang, Synthesis and characterization of novel forward osmosis membranes based on layer-by-layer assembly, Environ. Sci. Technol., 45 (2011) 5201–5208.

[11] M. Amini, M. Jahanshahi, A. Rahimpour, Synthesis of novel thin film nanocomposite (TFN) forward osmosis membranes using functionalized multi-walled carbon nanotubes, J. Membr. Sci., 435 (2013) 233–241.
[12] P. Zhong, X. Fu, T.-S. Chung, M. Weber, C. Maletzko, Development of thin-film composite forward osmosis hollow fiber membranes using direct sulfonated polyphenylenesulfone (sPPSU) as membrane substrates, Environ. Sci. Technol., 47 (2013) 7430–7436.
[13] P. Sukitpaneenit, T.-S. Chung, High performance thin-film composite forward osmosis hollow fiber membranes with macrovoid-free and highly porous structure for sustainable water production, Environ. Sci. Technol., 46 (2012) 7358–7365.
[14] R.C. Ong, T.-S. Chung, J.S. de Wit, B.J. Helmer, Novel cellulose ester substrates for high performance flat-sheet thin-film composite (TFC) forward osmosis (FO) membranes, J. Membr. Sci., 473 (2015) 63–71.
[15] N. Ma, J. Wei, S. Qi, Y. Zhao, Y. Gao, C.Y. Tang, Nanocomposite substrates for controlling internal concentration polarization in forward osmosis membranes, J. Membr. Sci., 441 (2013) 54–62.
[16] D.L. Shaffer, J.R. Werber, H. Jaramillo, S. Lin, M. Elimelech, Forward osmosis: where are we now?, Desalination, 356 (2015) 271–284.
[17] N.Y. Yip, A. Tiraferri, W.A. Phillip, J.D. Schiffman, M. Elimelech, High performance thin-film composite forward osmosis membrane, Environ. Sci. Technol., 44 (2010) 3812–3818.
[18] S. Chou, L. Shi, R. Wang, C.Y. Tang, C. Qiu, A.G. Fane, Characteristics and potential applications of a novel forward osmosis hollow fiber membrane, Desalination, 261 (2010) 365–372.
[19] N. Widjojo, T.-S. Chung, M. Weber, C. Maletzko, V. Warzelhan, The role of sulphonated polymer and macrovoid-free structure in the support layer for thinfilm composite (TFC) forward osmosis (FO) membranes, J. Membr. Sci., 383 (2011) 214–223.
[20] A. Sagle, B. Freeman, Fundamentals of Membranes for Water Treatment, The Future of Desalination in Texas, Texas Water Development Board, Austin, TX, 2004, pp. 137–154.
[21] B. Mi, M. Elimelech, Chemical and physical aspects of organic fouling of forward osmosis membranes, J. Membr. Sci., 320 (2008) 292–302.
[22] D. Emadzadeh, W. Lau, T. Matsuura, A. Ismail, M. Rahbari-Sisakht, Synthesis and characterization of thin film nanocomposite forward osmosis membrane with hydrophilic nanocomposite support to reduce internal concentration polarization, J. Membr. Sci., 449 (2014) 74–85.
[23] A. Nguyen, L. Zou, C. Priest, Evaluating the antifouling effects of silver nanoparticles regenerated by TiO_2 on forward osmosis membrane, J. Membr. Sci., 454 (2014) 264–271.
[24] N. Niksefat,M. Jahanshahi, A. Rahimpour, The effect of SiO_2 nanoparticles on morphology and performance of thin film composite membranes for forward osmosis application, Desalination, 343 (2014) 140–146.
[25] R. Wang, L. Shi, C.Y. Tang, S. Chou, C. Qiu, A.G. Fane, Characterization of novel forward osmosis hollow fiber membranes, J. Membr. Sci., 355 (2010) 158–167.
[26] A.B. Djurišić, X.Y. Chen, Y.H. Lung, Recent progress in hydrothermal synthesis of zinc oxide nanomaterials, Recent Pat. Nanotechnol., 6 (2012) 124–134.
[27] The International Centre for Diffraction Data (ICDD®) is a Non-Profit Scientific Organization Dedicated to Collecting, Editing, Publishing, and Distributing Powder Diffraction Data for the Identification of Materials, USA.
[28] M. Sairam, E. Sereewatthanawut, K. Li, A. Bismarck, A.G. Livingston, Method for the preparation of cellulose acetate flat sheet composite membranes for forward osmosis—desalination using $MgSO_4$ draw solution, Desalination, 273 (2011) 299–307.
[29] N. Srinivasa Rao, M.V. Basaveswara Rao, Structural and optical investigation of ZnO nanopowders synthesized from zinc chloride and zinc nitrate, Am. J. Mater. Sci., 5 (2015) 66–68.
[30] S. Ehsan, S. Mohtada, M.Toraj, Effect of preparation variables on morphology and pure water permeation flux through asymmetric cellulose acetate membranes, J. Membr. Sci., 326 (2009) 627–634.
[31] M. Mulder, Basic Principles of Membrane Technology, Kluwer Academic Publishers, Springer Nature, Switzerland, 1997.
[32] C.C. Pereira, R. Nobrega, C.P. Borges, Membrane formation with presence of Lewis acid–base complexes in polymer solution, J. Appl. Polym. Sci., 83 (2002) 2022–2034.
[33] M. Mulder Pervaporation, Separation of Ethanol-Water and of Isomeric Xilenes, Ph.D. Thesis, University of Twente, Enschede, Netherlands, 1984.
[34] R.C. Binning, R.J. Lee, J.F. Jennings, E.C. Martin, Separation of liquid mixtures by permeation, Ind. Eng. Chem., 53 (1961) 45–50.
[35] P. Aptel, J. Cuny, J. Jozefonvicz, G. Morel, J. Weel, Liquid transport through membranes prepared by grafting of polar monomers onto poly(tetrafluoroethylene) films. II. Some factors determining pervaporation rate and selectivity, Appl. Polym. Sci., 18 (1974) 351–364.
[36] M.M. Cipriano, Pervaporation and Desidratation of Organic Solvents—Preparation of Porous Layers for Composite Membranes, M.S. Thesis, Instituto Superior Técnico, Universidade Técnica de Lisboa, Lisboa, Portugal, 2001.
[37] R. Hong, T. Pan, J. Qian, H. Li, Synthesis and surface modification of ZnO nanoparticles, Chem. Eng. J., 119 (2006) 71–81.
[38] J. Garcia-Ivars, M. Iborra-Clar, M. Alcaina-Miranda, J. Mendoza-Roca, L. Pastor-Alcañiz, Development of fouling-resistant polyether sulfone ultrafiltration membranes via surface UV photografting with polyethylene glycol/aluminum oxide nanoparticles, Sep. Purif. Technol., 135 (2014) 88–99.
[39] A. Al-Hobaib, J. El Ghoul, L. El Mir, Fabrication of polyamide membrane reached by ZnO nanoparticles for ground water purification, Desal. Water Treat., 2015 (2015) 1–10.
[40] C. Liu, R. Bai, Preparation of chitosan/cellulose acetate blend hollow fibers for adsorptive performance, J. Membr. Sci., 267 (2005) 68–77.
[41] S. Waheed, A. Ahmad, S.M. Khan, S. Gul, T. Jamil, A. Islam, T. Hussain, Synthesis, characterization, permeation and antibacterial properties of cellulose acetate/polyethylene glycol membrane modified with chitosan, Desalination, 351 (2014) 59–69.
[42] A. Sonia, K. Priya Dasan, Chemical, morphology and thermal evaluation of cellulose microfibers obtained from *Hibiscus sabdariffa*, Carbohydr. Polym., 92 (2013) 668–674.
[43] M.K. Mohamad Haafiz, S.J. Eichhorn, A. Hassan, M. Jawaid, Isolation and characterization of microcrystalline cellulose from oil palm biomass residue, Carbohydr. Polym., 93 (2013) 628–634.
[44] Y. Yue, G. Han, Q. Wu, Transitional properties of cotton fibers from cellulose I to cellulose II structure, Bioresources, 8 (2013) 6460–6471.
[45] A.S. Abdel-Naby, A.A. Al-Ghamdi, Chemical modification of cellulose acetate by diallylamine, Int. J. Curr. Microbiol. Appl. Sci., 3 (2014) 10–24.
[46] Q. Li, Z. Xu, I. Pinnau, Fouling of reverse osmosis membranes by biopolymers in wastewater secondary effluent: role of membrane surface properties and initial permeate flux, J. Membr. Sci., 290 (2007) 173–181.
[47] J. Zheng, R. Ozisik, R.W. Siegel, Disruption of self-assembly and altered mechanical behavior in polyurethane/zinc oxide nanocomposites, Polymer, 46 (2005) 10873–10882.
[48] M.Z. Rong, M.Q. Zhang, H.B. Wang, H.M. Zeng, Surface modification of magnetic metal nanoparticals through irradiation graft polymerization, Appl. Surf. Sci., 200 (2002) 76–93.
[49] E. Tang, G. Cheng, X. Maa, X. Pang, Q. Zhao, Surface modification of zinc oxide nanoparticle by PMAA and its dispersion in aqueous system, Appl. Surf. Sci., 252 (2006) 5227–5523.
[50] H. Isawi, M.H. El-Sayed, X. Feng, H. Shawky, M.S. Abdel Mottaleb, Surface nanostructuring of thin film composite membranes via grafting polymerization and incorporation of ZnO nanoparticles, Appl. Surf. Sci., 385 (2016) 268–281.
[51] S. Malladi, B. Mallikarjunagouda, S. Ravindra, A. Sangamesh, M.A. Tejfaj, Novel dense poly(vinyl alcohol)-TiO_2 mixed matrix

membranes for prevaporation separation of water-isopropanol mixtures at 30°C, J. Membr. Sci., 281 (2006) 95–102.
[52] R. Augustine, H.N. Malik, D.K. Singhal, A. Mukherjee, D. Malakar, N. Kalarikkal, S. Thomas, Electrospun poly caprolactone/ZnO nanocomposite membranes as biomaterials with antibacterial and cell adhesion properties, J. Polym. Res., 21 (2014) 347.
[53] M. Moniruzzaman, J. Chattopadhyay, W.E. Billups, K.I. Winey, Tuning the mechanical properties of SWNT/Nylon 6, 10 composites with flexible spacers at the interface, Nano Lett., 7 (2007) 1178–1185.
[54] A. Rahimpour, S.S. Madaeni, S. Mehdipour-Ataei, Synthesis of a novel poly(amideimide) (PAI) and preparation and characterization of PAI blended polyethersulfone (PES) membranes, J. Membr. Sci., 311 (2008) 349–359.
[55] A. Rahimpour, S.S. Madaeni, Polyethersulfone (PES)/cellulose acetate phthalate (CAP) blend ultrafiltration membranes: preparation, morphology, performance and antifouling properties, J. Membr. Sci., 305 (2007) 299–312.
[56] J.F. Li, Z.L. Xu, H. Yang, L.Y. Yu, M. Liu, Effect of TiO_2 nanoparticles on the surface morphology and performance of microporous PES membrane, Appl. Surf. Sci., 255 (2009) 4725–4732.